Supporting information

Phase-controlled synthesis of Ni nanocrystals with high catalytic activity in 4-nitrophenol reduction

Jiahao Zhuang, ‡[ab] Xianglin Liu, ‡[c] Yongjun Ji,[bd] Fangna Gu[be] Jing Xu,[c] Yi-fan Han,[c] Guangwen Xu,[f] Ziyi Zhong,[g] Fabing Su*[bef]*

[a]School of Chemical Engineering, University of Chinese Academy of Sciences, Beijing 100049, China.
[b]State Key Laboratory of Multiphase Complex Systems, Institute of Process Engineering, Chinese Academy of Sciences, Beijing 100190, China.
[c]State Key Laboratory of Chemical Engineering, School of Chemical Engineering, East China University of Science and Technology, Shanghai 200237, China.
[d]School of Light Industry, Beijing Technology and Business University, Beijing 100048, China.
[e]Zhongke Langfang Institute of Process Engineering, Fenghua Road No 1, Langfang Economic & Technical Development Zone, Hebei 065001, China.
[f]Institute of Industrial Chemistry and Energy Technology, School of Chemical Engineering Shenyang University of Chemical Technology, Shenyang, Liaoning 110142, China.
[g]College of Engineering, Guangdong Technion Israel Institute of Technology (GTIIT), 241 Daxue Road, Shantou, 515063, China; Technion Israel Institute of Technology, (IIT), Haifa, 32 000, Israel.

J.Z. and X.L. contributed equally.

Corresponding Authors
* Fabing Su: fbsu@ipe.ac.cn
* Fangna Gu: fngu@ipe.ac.cn
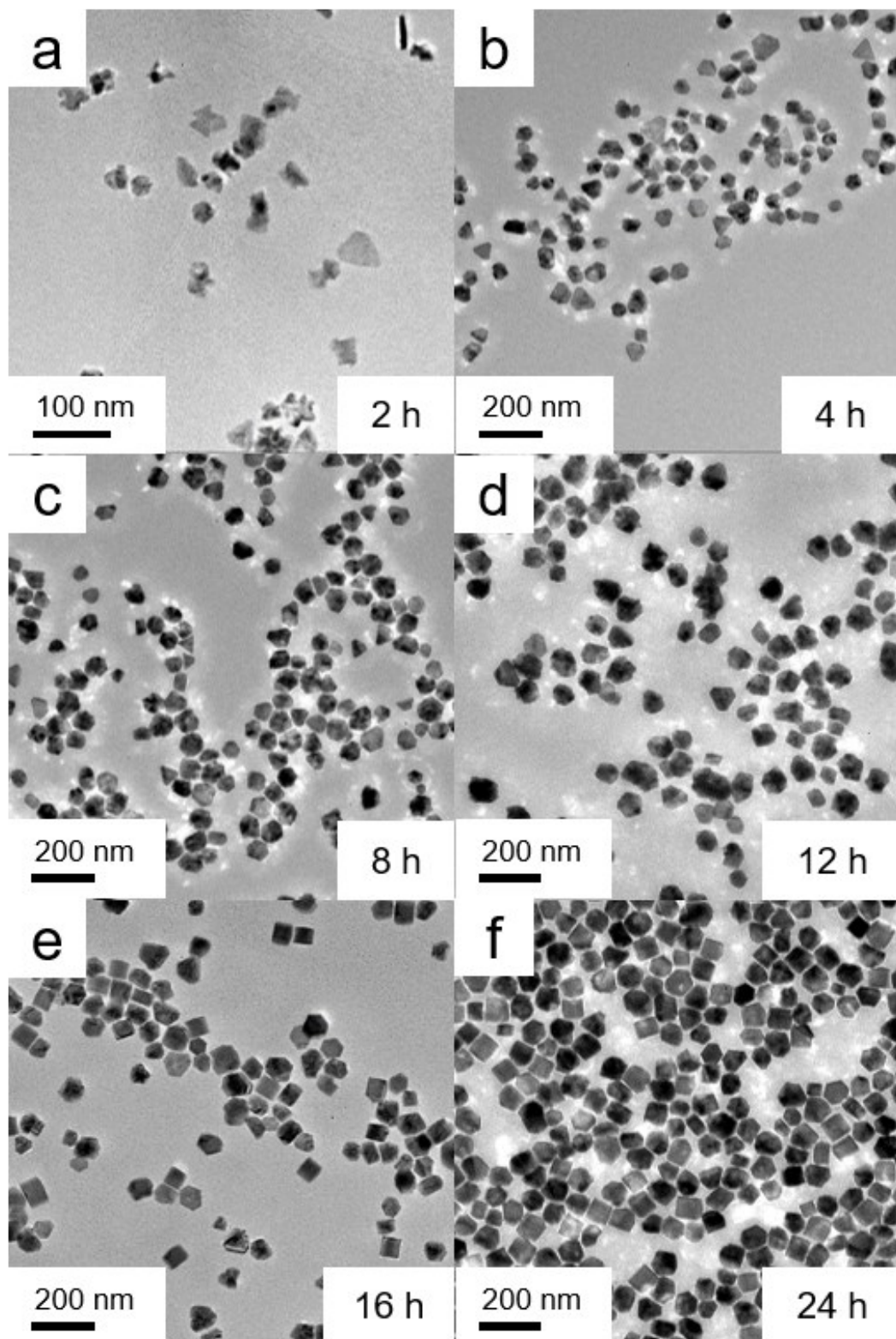
Fig. S1. TEM images of samples obtained in the typical synthesis of hcp-HP at reaction time of (a) 2 h, (b) 4 h, (c) 8 h, (d) 12 h, (e) 16 h and (f) 24 h.
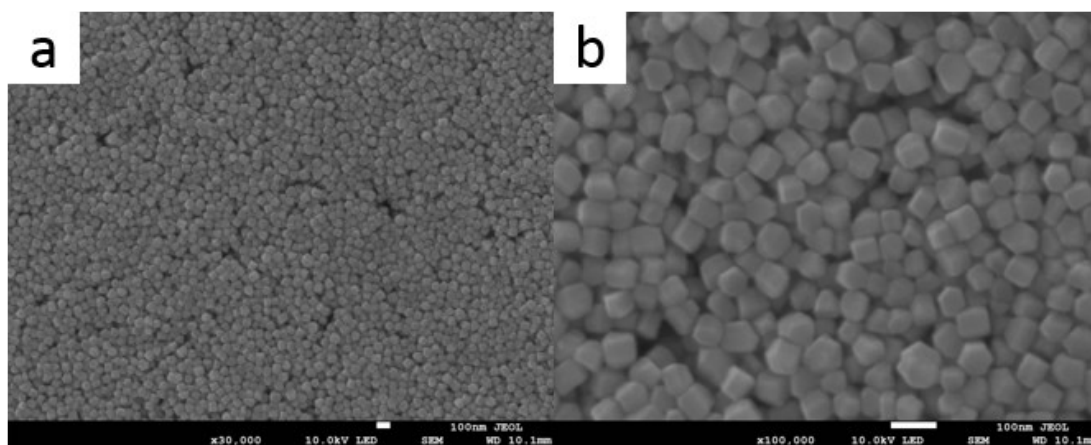
Fig. S2. (a) Low-magnification and (b) high-magnification SEM images of hcp-HP Ni NCs.
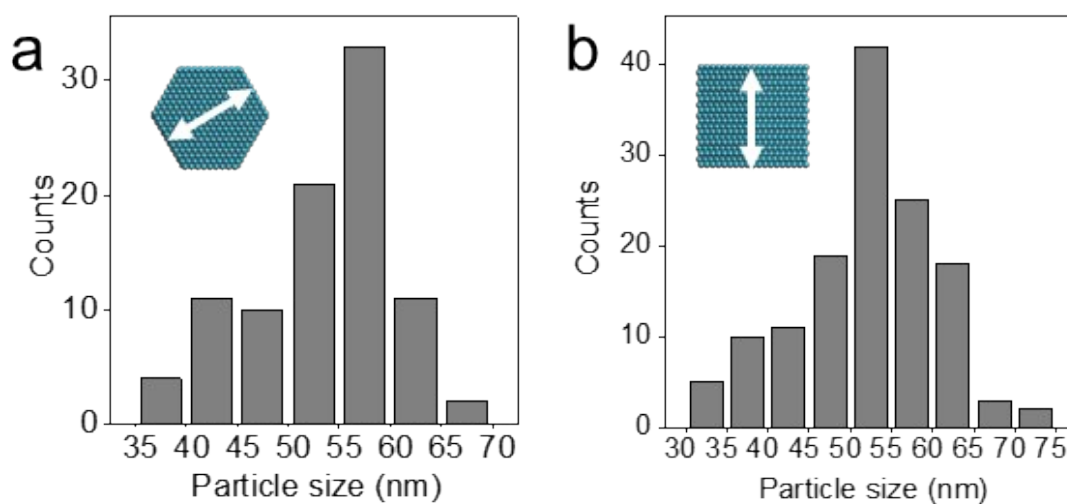
Fig. S3. Size distribution of hcp-HP Ni NCs: (a) hexagon and (b) oblong.
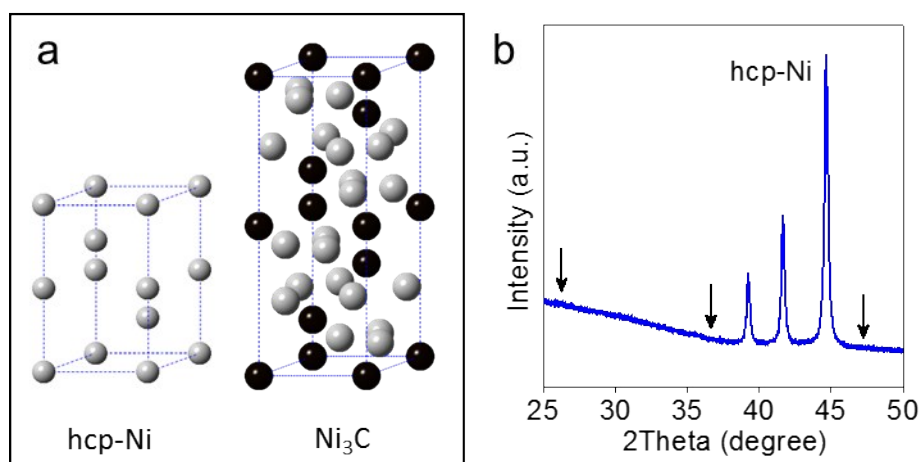
Fig. S4. (a) Crystal structures of hexagonal hcp-Ni and rhombohedral Ni₃C. (b) Higher-resolution scans of the XRD pattern of hcp-HP Ni NCs.
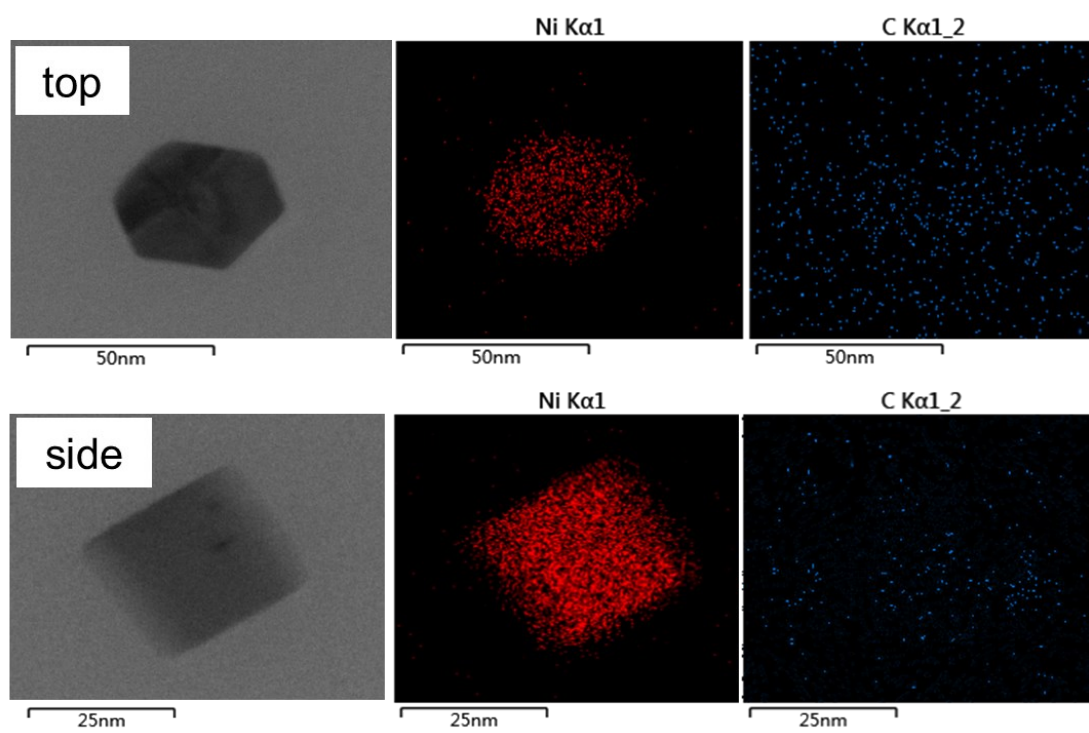
Fig. S5. EDS elemental mapping analysis of hcp-HP viewed from top and side.
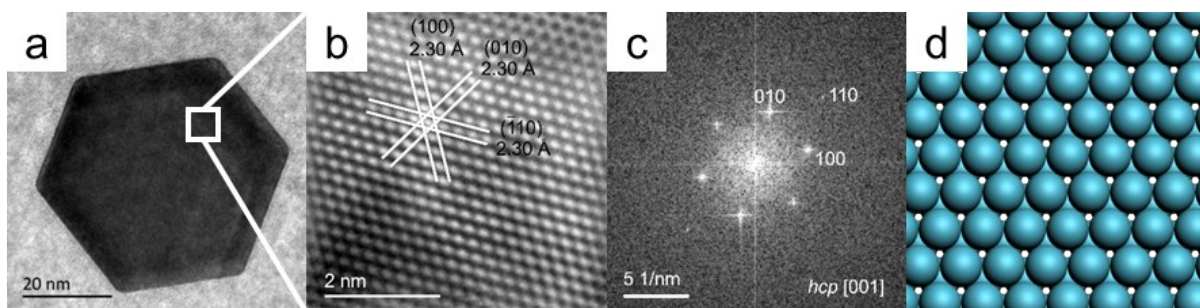
Fig. S6. (a) TEM, (b) HRTEM image, (c) FFT pattern and (d) atom stacking sequence of hcp-HP Ni viewed from top face.
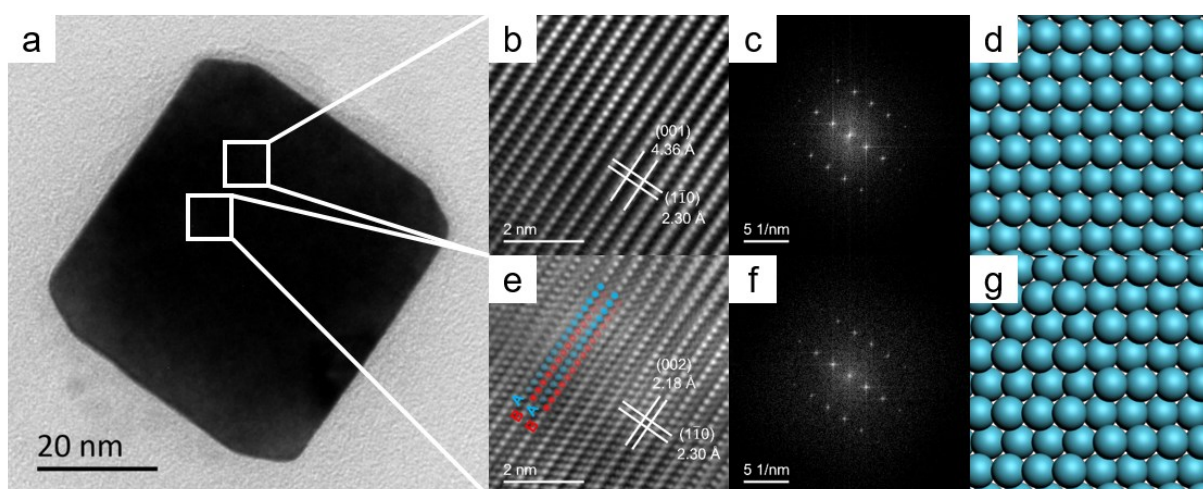
Fig. S7. (a) TEM of hcp-HP Ni NCs viewed along [110] zone axes. (b) HRTEM image, (c) FFT pattern and (d) atom layer stacking sequences of marginal area. (e) HRTEM image, (f) FFT pattern and (g) atom layer stacking sequences of middle area.
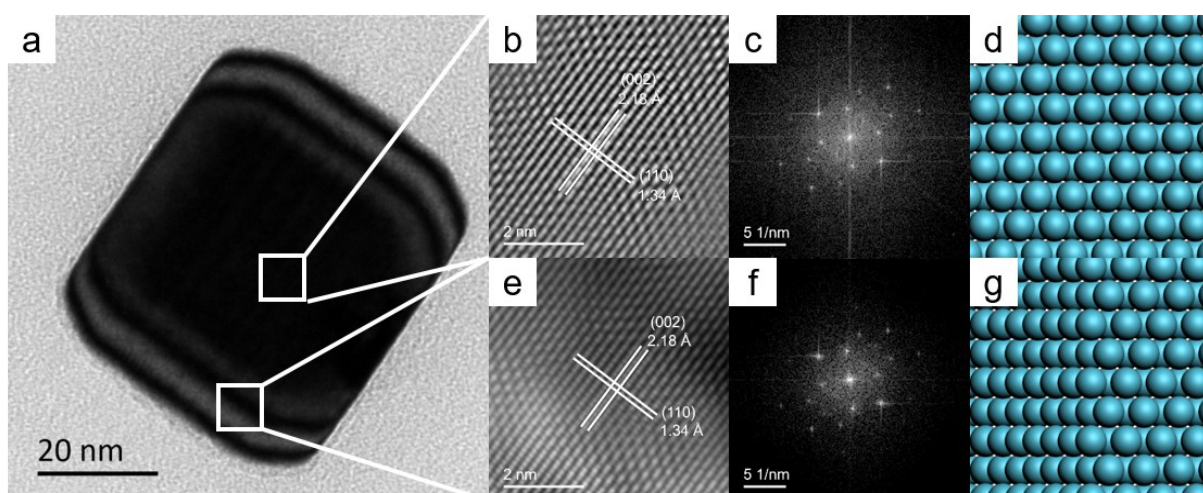
Fig. S8. (a) TEM of hcp-HP Ni NCs viewed along [100] zone axes. (b) HRTEM image, (c) FFT pattern and (d) atom layer stacking sequences of middle area. (e) HRTEM image, (f) FFT pattern and (g) atom layer stacking sequences of marginal area.
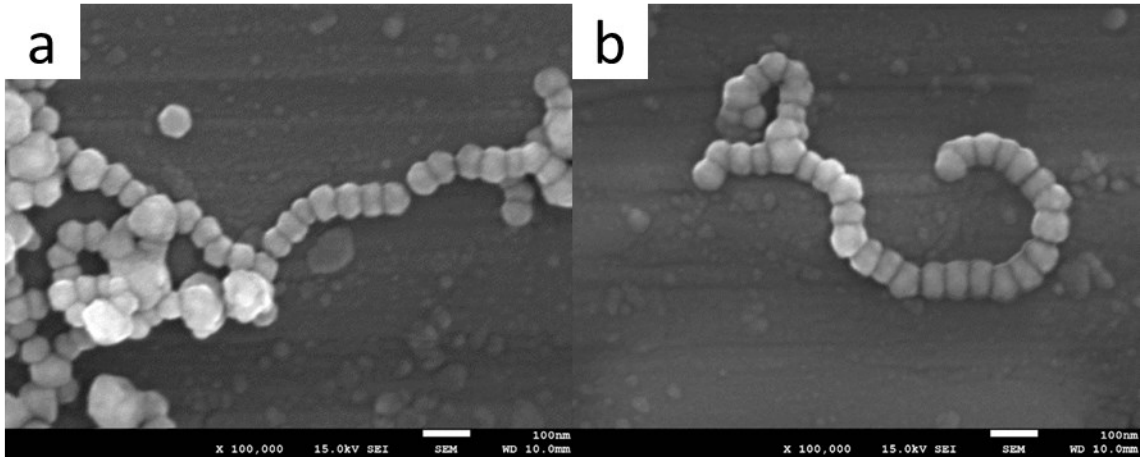
Fig. S9. (a, b) SEM images of fcc-IC Ni NCs.
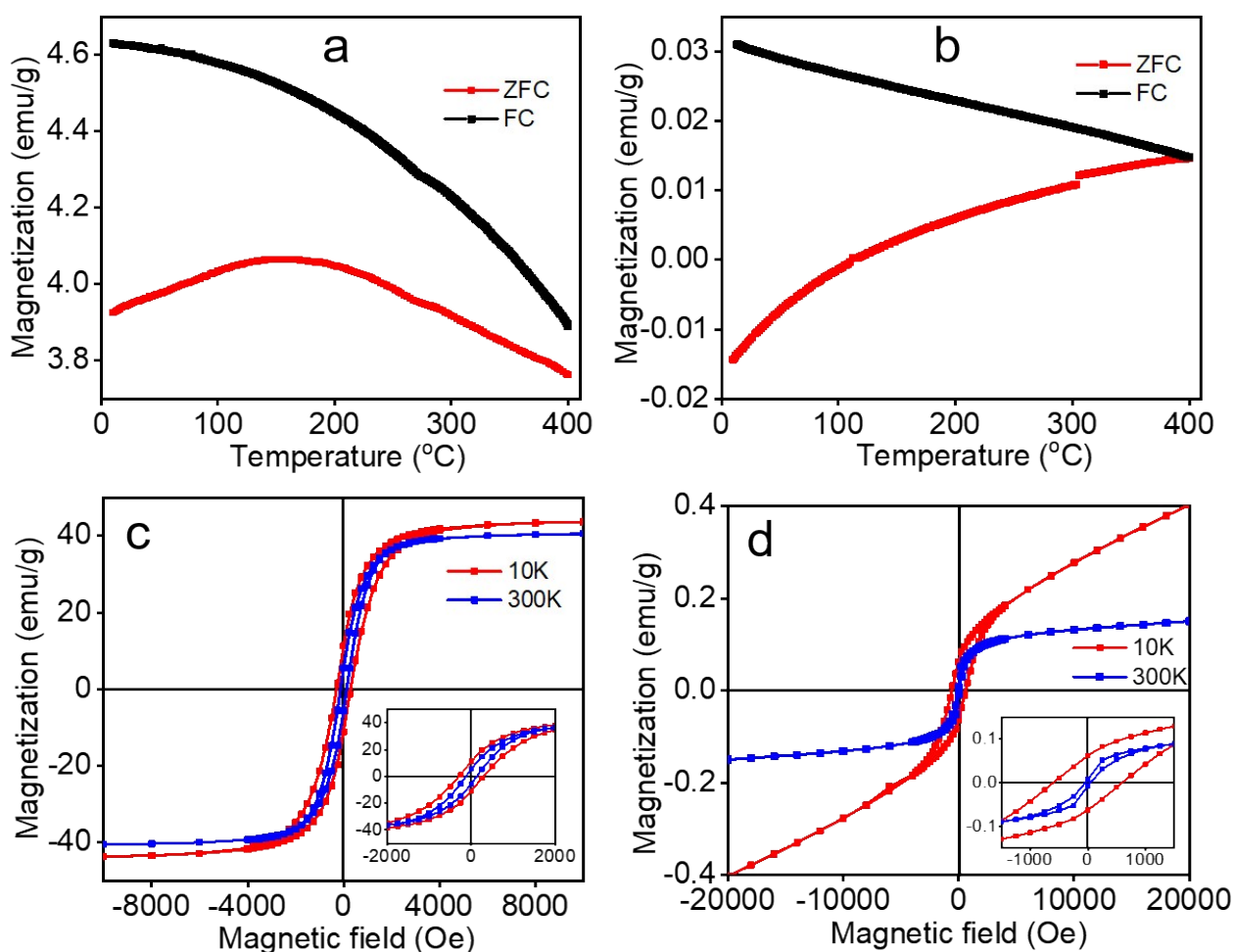
Fig. S10. (a) Zero-field cooling and field cooling (ZFC-FC) curves of fcc-IC Ni NCs. (b) ZFC-FC curves of hcp-HP Ni NCs. (c) Magnetization-magnetic field (M-H) plots of fcc-IC Ni NCs at 10 and 300 K. (d) M-H plots of hcp-HP Ni NCs at 10 and 300 K.

From the FC curve (2-400 K) of fcc-IC NCs (Fig. S10a), it can be seen that the magnetization increases with decreasing temperature, indicating its ferromagnetic property.[1] The disconnected ZFC-FC curves imply a high Curie temperature beyond the measuring range of the magnetometer, which is above 400 K. The bifurcated ZFC-FC curves (2-400 K) for the hcp-HP NCs (Fig. S10b) indicate that it is also ferromagnetic and its Curie temperature is also above 400 K. As can be seen in the magnetization-magnetic field (M-H) plots of fcc-IC and hcp-HP NCs at different temperatures (Fig. S10c and S10d, and insets), the coercivities (H_c) are 292 and 129 Oe for fcc-IC, and 592 and 51 Oe for hcp-HP Ni NCs at 10 K and 300 K, respectively, indicating that it is easier for hcp-HP to transform to the superparamagnetic state upon increasing temperature than fcc-IC. Furthermore, the saturation magnetization (M_s) and corresponding remanent magnetization (M_r) of fcc-IC are much higher than that of hcp-HP Ni NCs, demonstrating that the magnetic properties of the former are stronger than that of the latter.
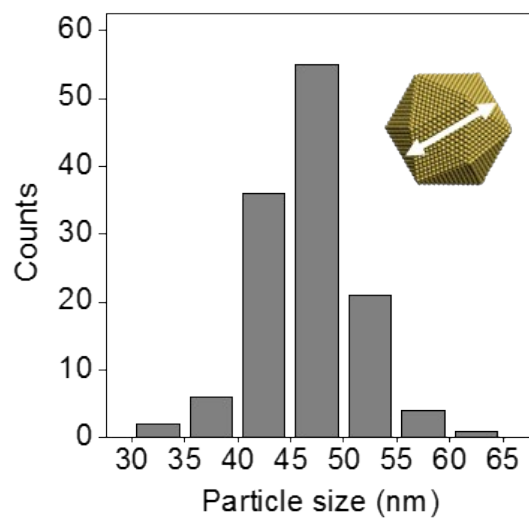
Fig. S11. Size distribution of fcc-IC Ni NCs.

Table S1. Average size of fcc-IC and hcp-HP Ni NCs.

Sample	Average size	
	By XRD (nm)	By TEM (nm)
fcc-IC	21.4	46.6
hcp-HP	46.5	52.7
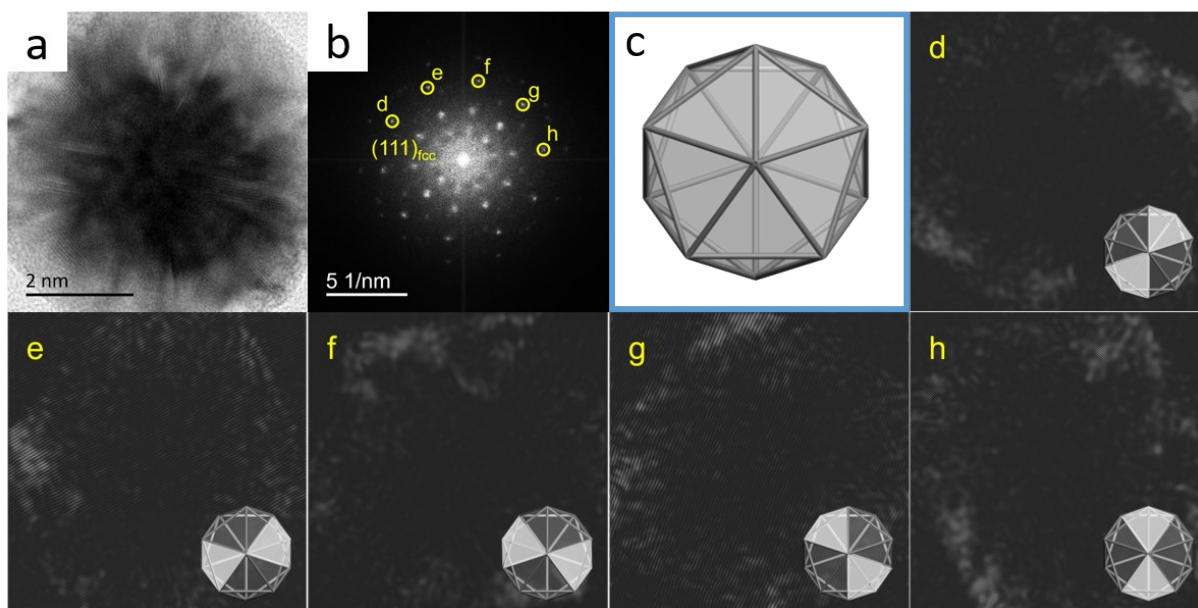
Fig. S12. (a) HRTEM and (b) FFT image of fcc-IC Ni NC viewed along fivefold twin symmetry axes. (c) Crystal structure modelling of five-fold symmetry icosahedral nanocrystal. (d-h) Transformed digital dark-field images by windowing different pairs of $(111)_{fcc}$ spots in the FFT image of (b).

In general, an icosahedral nanocrystal is formed by ten single-crystal tetrahedral units faceted with four $(111)_{fcc}$. To further illustrate its multiply twinned structure, transformed digital dark-field images were taken along the five-fold twin symmetry axes (Fig. S12). As shown in Fig. S12d-h, the bipyramid field was observed when a pair of the FFT spots corresponding to $(111)_{fcc}$ of the five-fold symmetric structure was converted imaged by the digital dark-field. These results clearly indicate that each spot corresponding to $(111)_{fcc}$ facet is the projection of two opposite tetrahedral subunits and further confirm the ten-fold twinned structure of fcc-IC Ni NCs.[2]
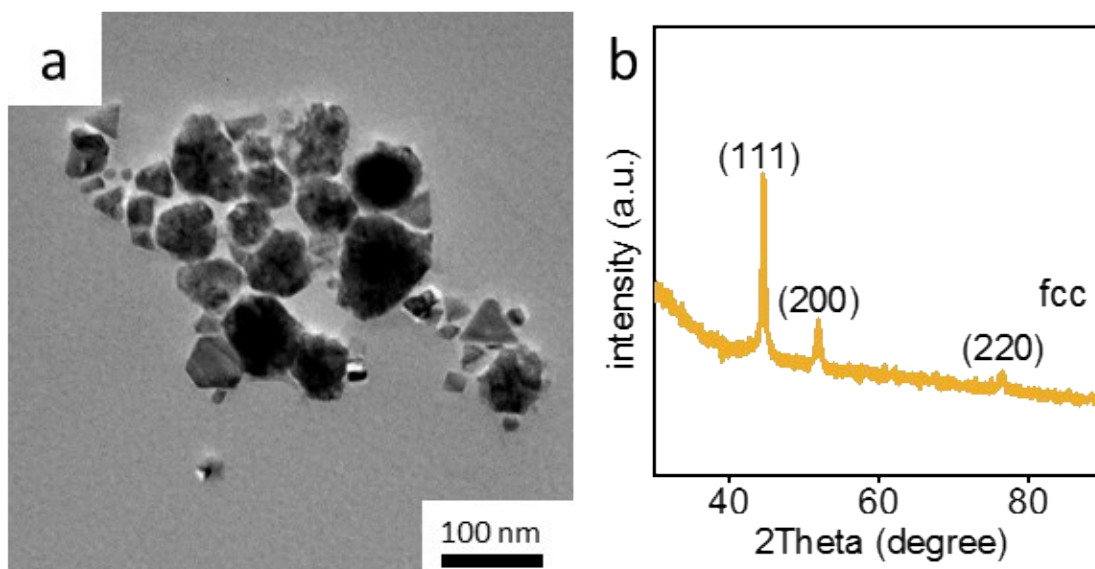
Fig. S13. TEM image and XRD pattern of Ni NCs obtained at relative high concentration of $[Ni^{2+}]$ without PEI.

Table S2. Computational results on the structures and energies for PEI molecules with the standing-up geometry adsorbed at the high-symmetry sites of fcc Ni(111), hcp Ni(001), (100), (101) and (102) facets.

Unit cell	facet	Initial site	Optimized site	d_{N-Ni} (nm)	E_{PEI} (eV)	E_{Ni} (eV)	$E_{PEI/Ni}$ (eV)	ΔE_{ads} (eV)	ΔE_{ads} (KJ/mol)
fcc	Ni(111)	top	top	0.21	-94.12	-125.96	-223.52	-3.44	-330.76
	Ni(111)	bridge	top	0.21	-94.12	-125.96	-223.51	-3.43	-329.79
	Ni(111)	hcp	top	0.21	-94.12	-125.96	-223.50	-3.42	-328.83
	Ni(111)	fcc	top	0.21	-94.12	-125.96	-223.52	-3.44	-330.76
hcp	Ni(001)	top	top	0.21	-94.12	-122.82	-220.45	-3.51	-337.49
	Ni(001)	bridge	top	0.21	-94.12	-122.82	-220.47	-3.53	-339.41
	Ni(001)	hcp	top	0.21	-94.12	-122.82	-220.43	-3.49	-335.56
	Ni(001)	fcc	top	0.21	-94.12	-122.82	-220.47	-3.53	-339.41
	Ni(100)	lower top	lower top	0.21	-94.12	-120.24	-217.63	-3.27	-314.41
	Ni(100)	higher top	higher top	0.20	-94.12	-120.24	-218.03	-3.67	-352.87
	Ni(100)	lower bridge	lower top	0.21	-94.12	-120.24	-217.63	-3.27	-314.41
	Ni(100)	stepped bridge	higher top	0.20	-94.12	-120.24	-218.05	-3.69	-354.79
	Ni(100)	higher bridge	higher top	0.21	-94.12	-120.24	-217.96	-3.60	-346.14
	Ni(101)	lower top	lower top	0.21	-94.12	-121.62	-219.13	-3.39	-325.95
	Ni(101)	higher top	higher top	0.21	-94.12	-121.62	-219.39	-3.65	-350.95
	Ni(101)	short bridge	higher top	0.20	-94.12	-121.62	-219.40	-3.66	-351.91
	Ni(101)	long bridge	lower top	0.21	-94.12	-121.62	-219.12	-3.38	-324.99
	Ni(101)	hcp	higher top	0.21	-94.12	-121.62	-219.30	-3.56	-342.29
	Ni(101)	fcc	higher top	0.20	-94.12	-121.62	-219.34	-3.60	-346.14
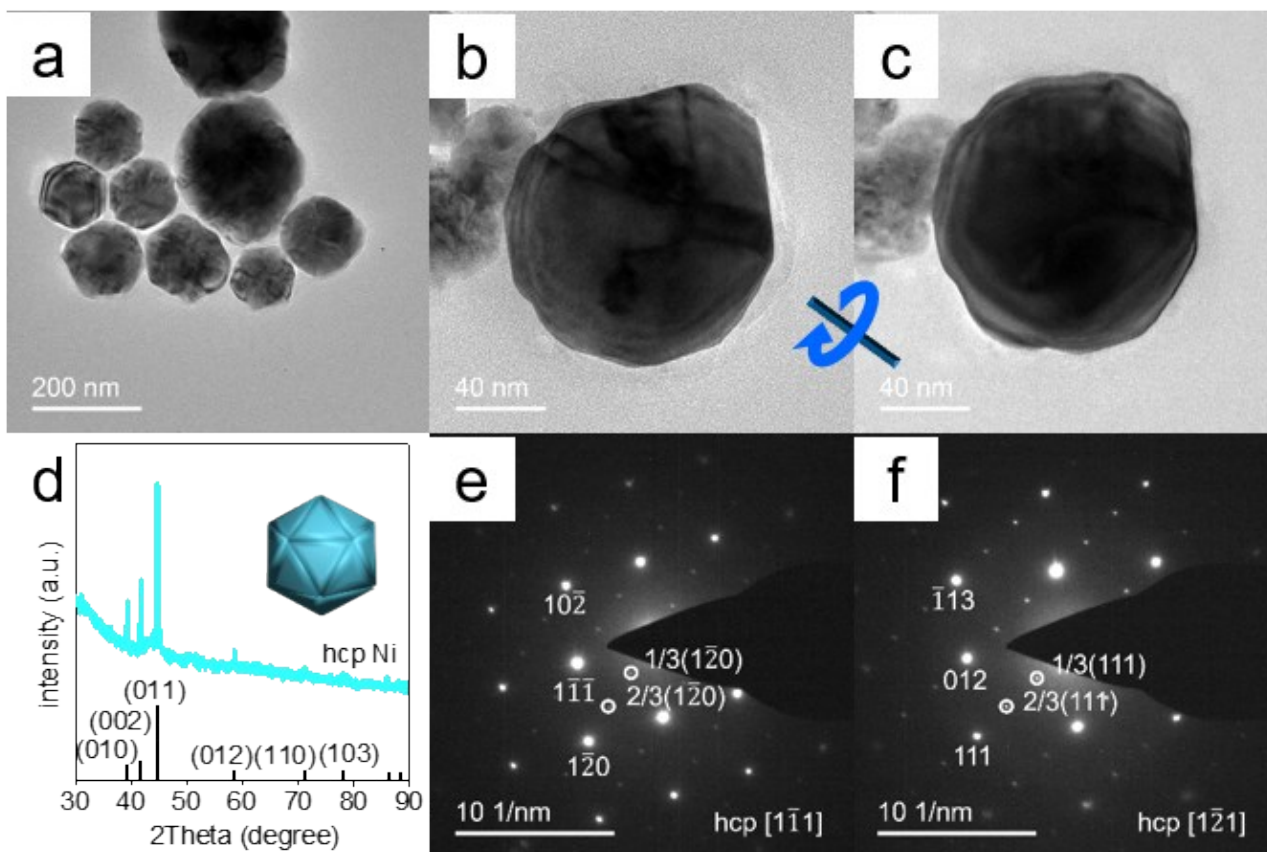
Fig. S14. Structure and detailed morphology analysis of icosahedron-like hcp Ni NCs. (a) Low-magnification and (b, c) high-magnification TEM images, (d) XRD pattern and (e, f) corresponding SAED patterns of the Ni NCs.

Fig. S14a displays the representative TEM image of icosahedron-like Ni NCs. XRD result (Fig. S14d) indicates a pure hcp phase (JCPDS-45-1027). The geometry was also identified by tilting experiments of TEM. By tilting a certain angle, similar hexagon-like NCs (Fig. S14b and S14c) were observed, indicating its icosahedron-like geometry. The corresponding SAED patterns (Fig. S14e and S14f) is consist of hcp Ni viewed along [1-11] and [1-21] directions.
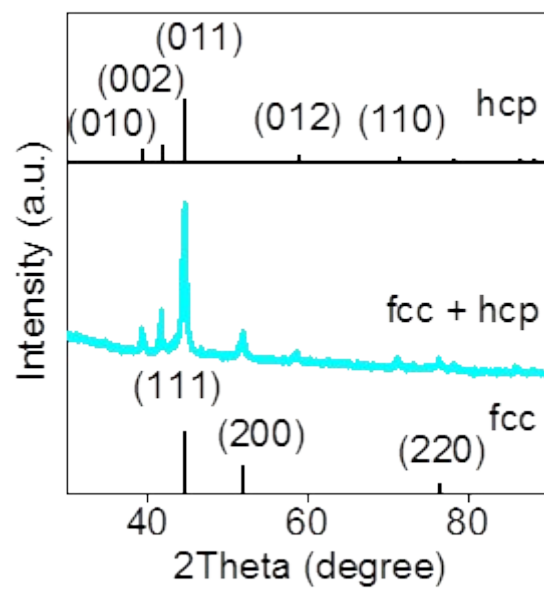
Fig. S15. XRD pattern of the product obtained at the reaction time of 84 h and 165 °C with Ni^{2+} concentration of 53.1 mM.
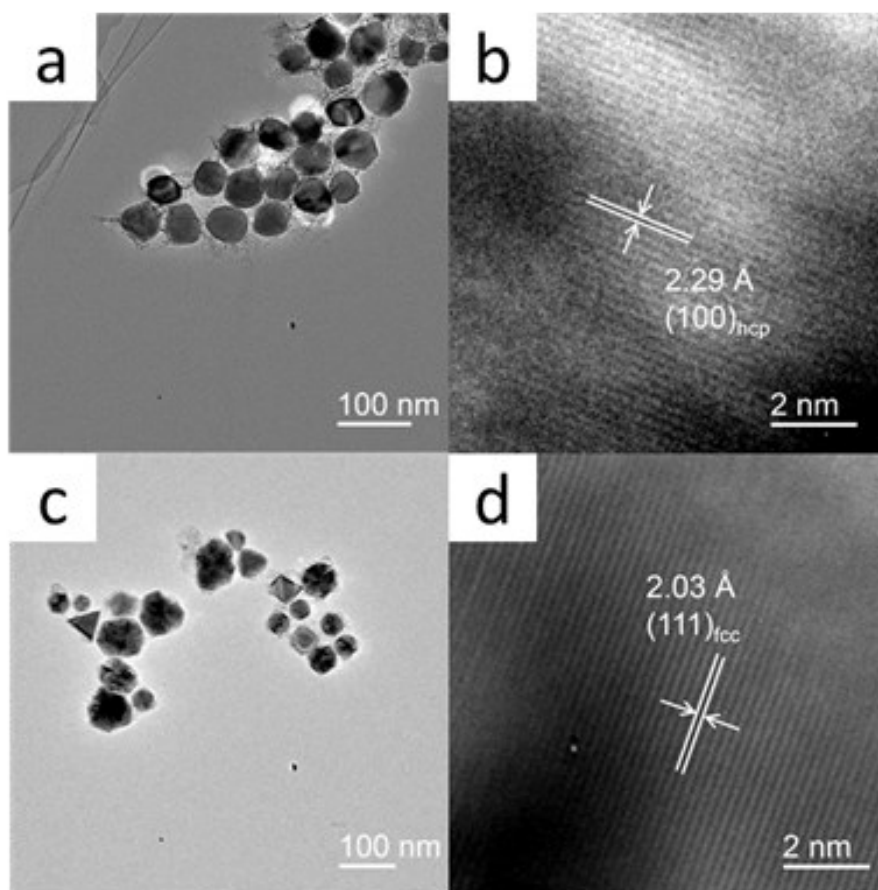
Fig. S16. TEM and HRTEM images of pre-reduced Ni NCs: (a, b) hcp-HP and (c, d) fcc-IC.
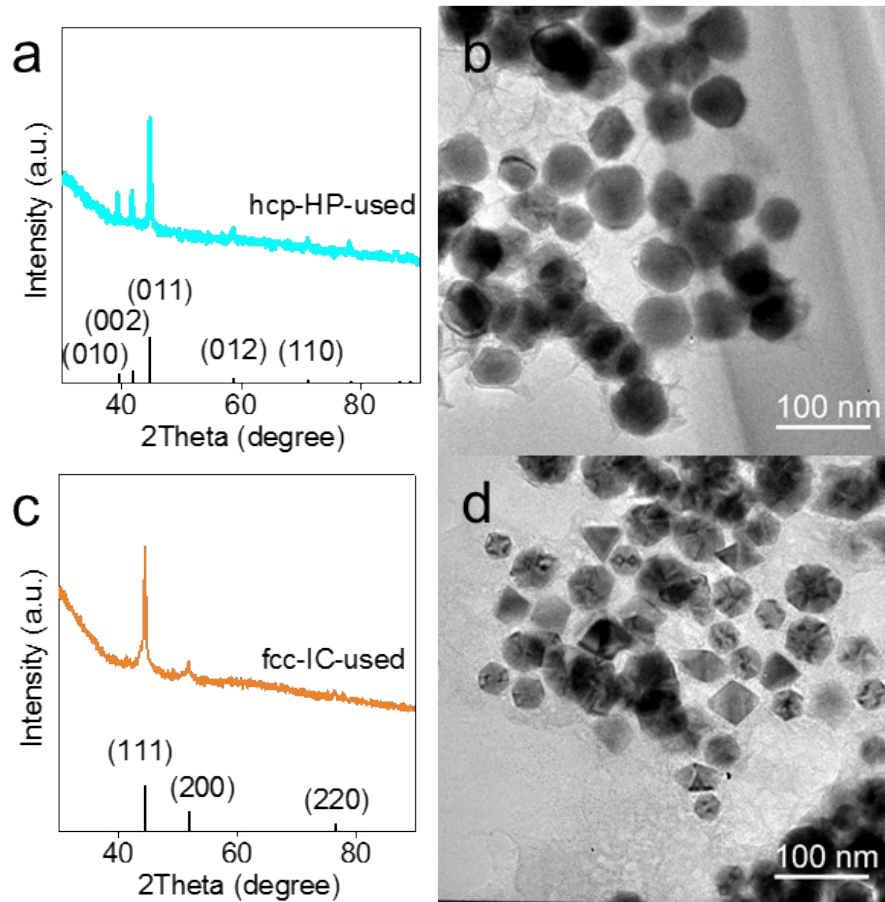
Fig. S17. XRD patterns and TEM images of used Ni catalysts: (a, b) hcp-HP; (c, d) fcc-IC.
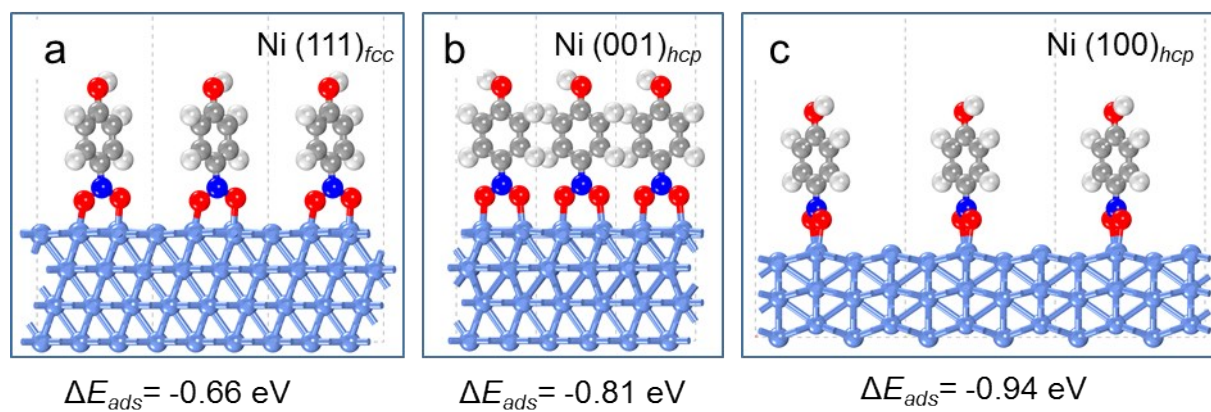
Fig. S18. Optimized structures of the adsorptions of 4-NP molecules on top site of: (a) fcc Ni(111), (b) hcp Ni(001), and (c) hcp (100) facets (from left to right) and the corresponding adsorption energy.

REFERENCES

1   M. Han, Q. Liu, J. He, Y. Song, Z. Xu and J. M. Zhu, *Adv. Mater.*, 2007, **19**, 1096-1100.

2   Z. X. Xie, W. C. Tzeng and C. L. Huang, *ChemPhysChem*, 2016, **17**, 2551-2557.